Effect of the 2021 Cumbre Vieja eruption on precipitable water vapor and atmospheric particles analysed using GNSS and remote sensing

MOKHAMAD NUR CAHYADI[1,2], ARIZAL BAWASIR[1], SYACHRUL ARIEF[3], AMIEN WIDODO[4], EKO YULI HANDOKO[1], PUTRA MAULIDA[1], SAIFUL AMAN HJ SULAIMAN[5], AMIR SHARIFUDDIN AB LATIP[5] AND ZAMBRI HARUN[6]

1 Geomatics Engineering Department, Institut Teknologi Sepuluh Nopember, Surabaya, Indonesia (cahyadi@geodesy.its.ac.id)

2 Research Center of Marine and Earth Science-Technology, Directorate of Research and Community Service, Institut Teknologi Sepuluh Nopember; Surabaya, Indonesia

3 Geospatial Education and Training Division, Geospatial Information Agency (BIG), Bogor, Indonesia

4 Department of Geophysics Engineering, Institut Teknologi Sepuluh Nopember; Surabaya, Indonesia

5 School of Geomatics Science and Natural Resources, College of Built Environment, Universiti Teknologi MARA, Shah Alam, Malaysia

6 Department of Mechanical and Manufacturing Engineering, Faculty of Engineering and Built Environment, Universiti Kebangsaan Malaysia, UKM Bangi, Malaysia

Received: August 25, 2023; Revised: Februaty 6, 2024; Accepted: February 26, 2024

ABSTRACT

The eruption of Mount Cumbre Vieja, La Palma, Spain, on 19th September 2021 released large amounts of gas and volcanic ash into the atmosphere that spread over hundreds of kilometers. Subsequently, the volumes of gaseous, and water vapor components in the troposphere were highly disturbed. In general, the release of a large amount of water vapor during an eruption increases the value of path delay and vertical column density of SO_2. Therefore, this study analyzed their variations to determine the impact of eruption. The precise point positioning on Global Navigation Satellite System (GNSS) observation data were processed to obtain zenith tropospheric delay (ZTD) and precipitable water vapor (PWV) contents, while Sentinel 5P, and MODIS remote sensing imagery were used to determine SO_2 column density, aerosol index, and surface temperature. Moreover, time series and correlation analysis were computed to analyze the effect of the eruption and the relationship between GNSS and remote sensing parameters. Our findings showed that the variations in precipitable water vapor affected the ZTD value for three GNSS stations around the eruption point, showing a correlation value above 0.98. Meanwhile, the remote sensing data indicated that the SO_2 content peaked at the end of September and in October 2021. Similarly, tropospheric delay, and water vapor had the highest fluctuations and

increases in the early eruption period. However, the lower atmosphere layer was generally influenced by the autumn climate. The content of particles released into the atmosphere during eruption had minor effect in the middle to the end of the eruption period as rainfall events led to an increase in water vapor. The surface temperature was found to be characterized mostly by autumn condition but showed fluctuations and increased values in the early period of the eruption.

K e y w o r d s : water vapor, GNSS, atmospheric particles, remote sensing, Cumbre Vieja, eruption

1. INTRODUCTION

The Global Navigation Satellite System (GNSS) utilizes radio signals for navigation and positioning purposes (*Seeber, 2003*). However, the signals transmitted from these GNSS satellites experience a delay or slowdown time when passing through the atmosphere due to the spatial and temporal processes and dynamics of the atmosphere (*Karabatić, 2011*). Thus, many studies have applied the GNSS signal delay as a parameter in determining the spatial and temporal characteristics of the atmosphere through the concept known as the GNSS inversion (*Bevis et al., 1992*).

In addition to the variations in the gas content of the atmosphere, the ashes from volcanic eruptions also contribute to the GNSS signal delay (*Larson, 2013*). The magnitude of this delay depends on the size (standard diameter does not exceed 4 mm) and density of ash particles. Note that the GNSS signal delay is assumed to be negligible for practical navigation purposes. However, some troposphere studies on volcanoes have showed that large amounts of water vapor released during volcanic eruptions generally increase the estimated path delay of GNSS, indicating that this sudden variation can be analyzed to determine the impact of volcanic eruptions (*Grapenthin et al., 2018*). This is a feasible analysis as volcanic eruptions inject tons of solid particles and gases transported across the atmosphere over minutes, weeks, or even years, depending on the altitude of the injection (*Robock et al., 2000*). After water vapor and carbon dioxide (CO_2), the next most abundant gas involved in volcanic activity is SO_2. These substances can easily be detected in areas isolated from anthropogenic sources, specifically SO_2 as it has a low concentration in the atmosphere (*Shinohara et al., 2008*). The collection of data on the predominant particle and gas content in an eruption is useful in monitoring volcanic activities to better understand the hazards and make efforts to reduce the associated risks (*Cofano et al., 2021*).

Larson (2013) introduced a method to detect volcanic plumes using the signal-to-noise ratio (*SNR*). This approach detects volcanic ash columns based on a phase-to-noise carrier density ratio. *Grapenthin et al. (2013)* also proposed a post-fit phase residual (*PPR*) method based on the difference between the observed and estimated phase distance measurements. This study also found that the instantaneous offset in positioning is correlated with volcanic explosive eruptions. Nevertheless, both the *PPR* and *SNR* approaches have limited applications due to the impact of unknown weather conditions. In addition, these approaches assume that the detected residue is mainly caused by volcanic ash without identifying any other rising gas and particulate matter in the atmosphere. Moreover, these methods were applied to well-understood volcanic activities, whereas our study presents

a case study of a volcano with strombolian eruption. A study by *Cahyadi et al. (2024)* monitored the content of water vapor and atmospheric particles in the same type of eruption, namely the eruption of Mount Semeru in December 2021. The difference between the two eruptions is in the characteristics of the climate and atmosphere. Where the study area on Mount Semeru is close to the equator with a two-season climate. Meanwhile, the study area of Mount Cumbre Vieja on La Palma Island has the characteristics of a subtropical climate (4 seasons). The 2021 Cumbre Vieja eruption which has a period of 3 months has the potential to have an influence on atmospheric activity during autumn in the study area.

The volcanic activity in La Palma has concentrated in the southern part of the island in the last 125000 years, mainly along the Cumbre Vieja volcanic ridge where eruptive vents and fissures align with the volcano's crest to form a distinctive marine island rift zone which is locally known as "dorsal". Moreover, the core of the rift zone, located beneath the aligned cinder cones and associated deposits at the surface, is created by dense swarms of embankments that represent feeder channels to the surface vents and cinder cones. In early September 2021, the intrusion of one of these dykes led to the opening of the erupting vent a few minutes after 14:00 local time on 19th September 2021 in the Cabeza de Vaca area on the west side of the Cumbre Vieja ridge (*Carracedo et al., 2022*). The series of Cumbre Vieja eruption activities was officially declared to end on 25th December 2021, after 12 days without any volcanic event. The water content in the area was found to be dominated by SO_2 gas and aerosol particles, and this further led to cloud cover at the eruption point and its surroundings (*Bennis and Venzke, 2021*). The SO_2 content and precipitable water vapor (*PWV*) are tropospheric parameters that are measured using different sensors and wavelengths. In the case of this eruption, significant increase in SO_2 has the potential to make larger particles in the form of sulphate aerosols (SO_4). This allows for the potential for a significant correlation between *PWV* and aerosol content in the atmosphere during the eruption period because aerosols can act as the center of water vapor condensation and affect cloud formation in the process of binary homogeneous nucleation (*Mirabel and Katz, 1974*; *Lachatre et al., 2022*).

This study is developed based on the need to comprehensively understand the dynamic relationship between volcanic activities, atmospheric conditions, and navigation systems, using Global Navigation Satellite System (GNSS). Specifically, volcanic eruptions introduce additional complexity to the initial delay due to signal propagation through the troposphere. The gases and particles emitted, including SO_2, affect GNSS signal delay, providing an opportunity for insightful analysis (*Larson, 2013*; *Grapenthin et al., 2018*). However, existing methodologies, such as *PPR* and *SNR*, have limitations by exclusively attributing residues to volcanic ash and neglecting other atmospheric factors. Based on this phenomenon, the eruption of Mount Cumbre Vieja in 2021 was investigated as a case study of a strombolian eruption with distinct climate and atmospheric characteristics. The significance of the investigation is dependent on the potential influence of volcanic activities on tropospheric parameters, including Zenith Total Delay (*ZTD*) and *PWV*, as well as the associated temporal variations in surface temperature, gas components, and aerosol particles.

This study aimed to determine the value of *ZTD* and water vapor content of *PWV* in the atmosphere using GNSS observation data. The analysis was carried out to evaluate the time-series fluctuations of tropospheric parameters, including the effects on the time before and

after the eruption of the Mount Cumbre Vieja in 2021. Additionally, temporal variations in surface temperature, dominant gas components, and aerosol particles in the Cumbre Vieja eruption area were analyzed using remote sensing data, and the results were correlated with GNSS observations. Through this correlation, the results are expected to show the intricacies of the 2021 Cumbre Vieja eruption, providing valuable insights for both scientific understanding and practical applications in atmospheric monitoring as well as hazard mitigation.

2. METHODOLOGY

2.1. GNSS-derived ZTD and PWV

2.1.1. General concept of ZTD and PWV

The *ZTD* parameter represents the time changes observed in GNSS satellite signals, passing through the tropospheric atmosphere to receiving stations on the Earth's surface (*Bevis et al., 1992*). As GNSS signals traverse the Earth's surface, specifically through the tropospheric layer, significant changes are observed in light speed and electromagnetic wave propagation, as shown in Fig. 1. Precision GNSS monitoring can be used to measure the time difference caused by *ZTD*. This information is crucial for determining the correction needed in the satellite-receiver-station distance measurement, ensuring accurate position determination.

The *PWV* parameter, derived from GNSS observations, is the quantity of atmospheric water vapor above the GNSS receiving station that can be calculated according to the change in *ZTD*. Based on the data obtained, the amount of *PWV* above the receiving station is estimated through the mathematical relationship between *ZTD* and water vapor content in the atmosphere. This *PWV* estimation plays a significant role in weather monitoring and

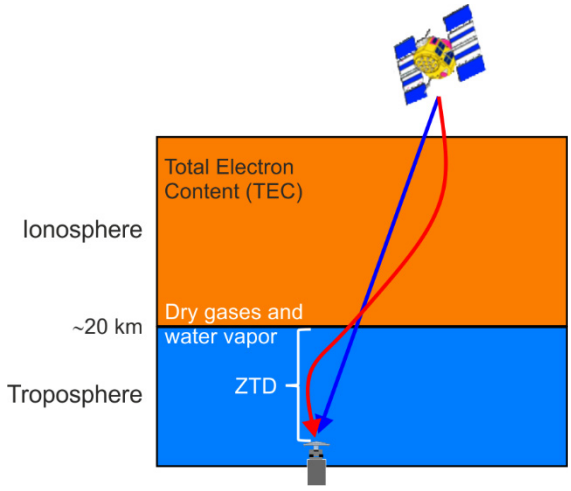

Fig. 1. Scheme of the GNSS signal delay in the atmosphere

climate, facilitating the understanding of the spatial and temporal distribution of atmospheric water vapor (*Bevis et al., 1994*).

2.1.2. ZTD and PWV data used in this study

The *ZTD* and *PWV* values were determined using the MAGNET GPS Network tropospheric data sourced from the Nevada Geodetic Laboratory at a frequency of 30 s. Meanwhile, the GNSS observations were processed using the precise point positioning (PPP) method that considered undifferenced observations from a single GNSS receiver. The PPP used IGS and UNAVCO absolute receiver and satellite antenna phase offsets at different values for the antenna model specified in the submitted observation file. The relative antenna phase center information was applied as the default. In addition, the data for the satellite antenna phase offsets and the phase center antenna used for the processing were downloaded in the form of an IGS antenna correction file through the CDDIS NASA website. The tropospheric data at stations around the study area were calculated at the source using the GipsyX-1 software that required the RINEX observation data, ephemeris data, clock, and IONEX as the main inputs. Moreover, the projection of the slant path delay value into a zenith delay was determined using the VMF1 mapping function. These analyses provided the following outputs: total/wet zenith tropospheric delay, gradients, precipitable water vapor, and mean surface temperature with a sampling rate of 300 s.

The MAZO and LPAL (La Palma Island) GNSS stations were considered in this study as they are the closest to the eruption site. The GOM1 (La Gomera Island) station was also considered for comparison of meteorological characteristics in locations around the site (Fig. 2).

The tropospheric delay is simulated in the direction of the zenith and later extended towards the satellite using a mapping function. This function is not solely based on the

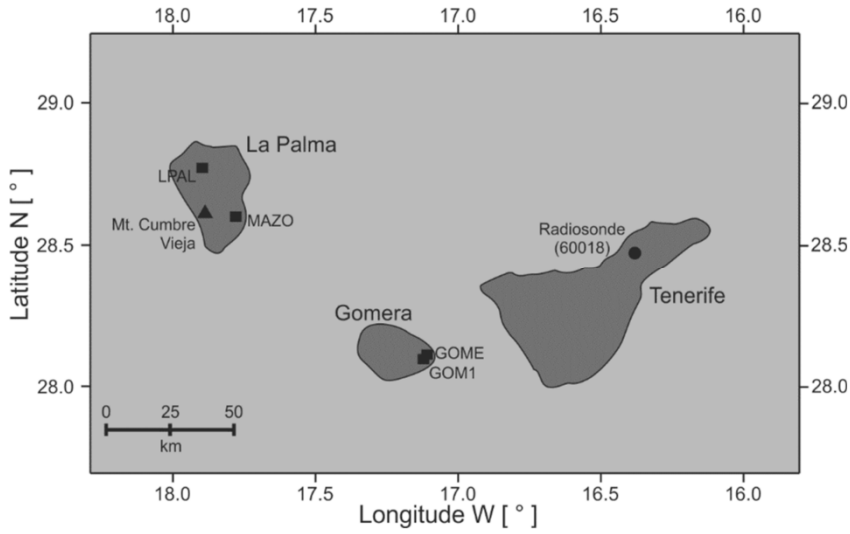

Fig. 2. Locations of the GNSS stations used to obtain the *ZTD* and *PWV* values.

elevation angle, as indicated by a simplified representation, but can also be influenced by various atmospheric factors. The zenith wet delay (*ZWD*), referred to as the non-hydrostatic component, is linked to the vertical arrangement of water vapor in the troposphere. Conversely, the dry component is known as the hydrostatic component (zenith hydrostatic delay - *ZHD*) of the total delay (*Bevis, 1992*):

$$ZTD = ZHD + ZWD\,. \tag{1}$$

The *ZHD* values were calculated using the Saastamoinen model (*Bevis, 1994*), based on the co-located surface meteorological data. The *ZWD* values were obtained by subtracting *ZHD* from *ZTD* (Eq. (1)). By using the empirical equation, *PWV* were obtained by multiplying the *ZWD* by the conversion factor (*Q*):

$$PWV = Q \cdot ZWD\,, \tag{2}$$

where

$$Q = \frac{1\times10^{-6}}{\rho_w\left(\dfrac{k_3}{T_m} + k_2'\right)R_v}\,, \tag{3}$$

with

$$T_m = 70.2 + 0.72T_s\,. \tag{4}$$

Here, ρ_w is density of water; k_2' and k_3 are atmospheric refraction constants with the empirical values of 22.13 ± 2.20 and $(3.739 \pm 0.012) \times 10^5$ K hPa^{-1}, respectively; $R_v = 461.495$ J kg^{-1} K^{-1} is gas constant of water vapor; T_m stands for weighted mean temperatue and T_s is land surface temperature.

2.2. SO_2 content, aerosol index, and land surface temperature

The SO_2 content and UV aerosol index (*UVAI*) data were obtained from Sentinel-5P imagery through Google Earth Engine. The vertical column density SO_2 data on the TROPOMI Sentinel-5P sensor was found to have a temporal resolution of one day. This facilitated the daily spatial monitoring of the SO_2 content in the troposphere. However, this sensor is associated with sensitive wavelengths at 340 and 380 nm, that are affected by clouds and can cause incomplete daily data.

The *UVAI* or absorbing aerosol index (*AAI*) used wavelengths in Rayleigh scattering in the UV spectral range to show the ratio or difference between the observed and modeled reflectance. A positive value indicates the presence of UV-absorbing aerosols, such as dust, smoke, and volcanic ash (as in this case). Moreover, Terra-MODIS level-3 data was used to identify surface temperatures during the eruption period using the Google Earth Engine platform. The T_s data can be affected by cloud cover, indicating that some pixels (in Google Earth engine land surface temperature imagery) may have a null value at a certain time.

2.3. Pixel value extraction of remote sensing data

Pixel values were extracted to determine the values of SO_2 content, aerosol index, and T_s at the pixels corresponding to the location of the GNSS station. Those remote sensing satellite imagery data was obtained through the Google Earth Engine geospatial processing service, which provides a cloud-based set of remote sensing satellite imagery data. The remote sensing data were obtained by determining the region of interest according to the study area, then date filtering according to the Cumbre Vieja eruption period. Daily data during the eruption period were downloaded in raster format. Values of the remote sensing data were obtained using ArcGIS 10.8 software by extracting pixel values (from raster files) according to the coordinates of the GNSS station locations. Resampling will not be applied to the input rasters in accordance with the analysis environment. Rather, cell values will be obtained from the original resolution and spatial reference of all input rasters. This is achieved by aligning input locations with the spatial reference of the raster to extract values. The pixel values extracted in this manner served as time-series data for remote sensing analysis during the eruption phase.

The pixel values obtained were used for temporal visualization and correlation analysis using *PWV* and *ZTD* content generated from GNSS data for the study area. Moreover, time series data previously obtained were adjusted by calculating their average to determine the correlation. The correlation method used in this research is Pearson's correlation. This method is usually used to measure linear relationships between continuous variables, which in this case are tropospheric parameters (*Guo et al., 2021*; *Wei et al., 2021*; *Kundu et al., 2022*).

2.4. Additional data

2.4.1. ERA5 atmospheric reanalysis

The ERA5 Atmospheric Reanalysis is a global climate data product produced by the European Center for Medium-Range Weather Forecasts (ECMWF, *https://confluence.ecmwf.int/display/CKB/ERA5%3A+data+documentation*). The data used for analysis in ERA5 are obtained from various sources, including satellites, surface observations, and atmospheric data. Subsequently, these data are entered into a numerical weather model to produce spatially and temporally consistent data. In this study, the "Total Precipitation" parameter was used as ERA5 atmospheric variable, containing hourly data at longitude-latitude grid 0.25° × 0.25° with single level pressure type. This parameter is the accumulated liquid and frozen water, including rain and snow, that falls to the Earth's surface, serving as the sum of large-scale and convective precipitation. Large-scale precipitation is generated by the cloud scheme in the ECMWF Integrated Forecasting System (*Hersbach et al., 2022*). The total precipitation data in this study is used to determine the rain conditions during the 2021 Cumbre Vieja eruption period, which occurred in the autumn.

2.4.2. Radiosonde data

The radiosonde data used in this study are obtained from Atmospheric Sounding provided by the University of Wyoming, which hosts a website showing the latest radiosonde observations (*http://weather.uwyo.edu/upperair/sounding.html*). The data

comprise of 1312 stations globally and the information provided is in the form of meteorological parameters, both in pressure and single level. Each station produces meteorological information at a temporal resolution of every 12 hours. Subsequently, the precipitable water parameter (single level) is used as supporting data to determine the difference between direct observation and calculation results from GNSS observation data. The closest radiosonde station to the eruption location is situated on Tenerife Island, which is approximately 150 km from the Mount Cumbre Vieja (Station Number 60018).

3. RESULTS

3.1. Zenith tropospheric delay

3.1.1. ZTD results at two stations

The patterns of *ZTD* values at MAZO and LPAL stations have similar characteristics (Fig. 3). As shown in Figs 3 and 4, fairly smooth values were recorded at the nearest GNSS station, MAZO, from early September to before the eruption started. The significant perturbation at the two stations became evident after the eruption started on 19th September.

The MAZO station, which was closer to the eruption point, showed a sharp perturbation in its values in six short periods of 22nd–23rd September, 26th–28th September, 4th October, 5th–6th November, 24th–26th November and 8th–9th December. Some of these periods are correlated with an increase in the value of aerosol optical depth (*AOD*) at the observation station in La Palma. Moreover, the increase in *ZTD* on 22nd September (3 days after the

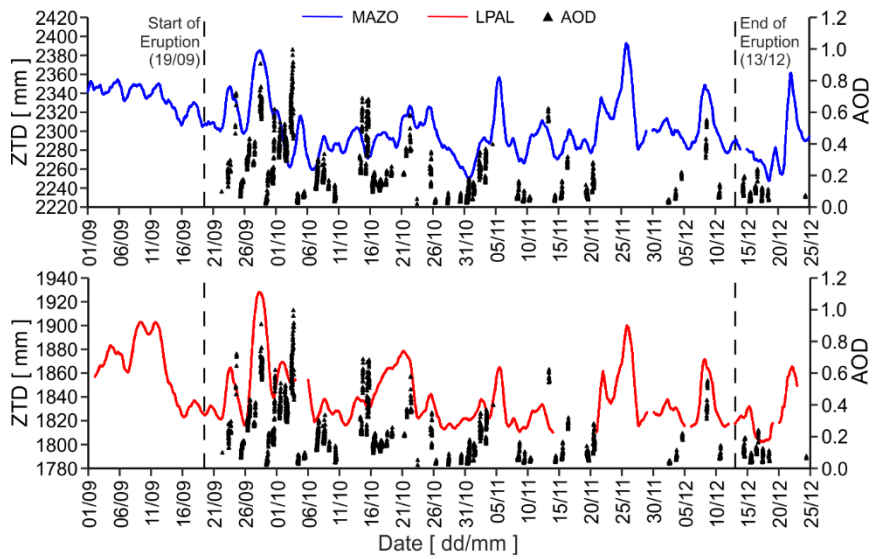

Fig. 3. Zenith tropospheric delay (*ZTD*) at MAZO and LPAL stations during the Cumbre Vieja eruption period.

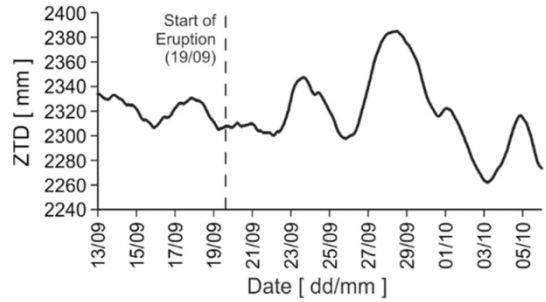

Fig. 4. Zenith tropospheric delay (*ZTD*) at the MAZO station during the early eruption period.

eruption) was directly proportional to the increase in aerosol concentrations in the atmosphere.

The GNSS data showed that the *ZTD* value and water vapor content at both MAZO and LPAL stations decreased and stagnated 2–3 days after the eruption. This is possibly due to the occurrence of volcanic eruptions that heat the troposphere and reduce the density of the atmosphere, causing the GPS signals passing through the troposphere to propagate faster than normal. This is similar to the decrease detected in the tropospheric delay at the beginning of the eruption in Mount Chaiten, Chile in 2009 (*Akilan et al., 2019*).

3.1.2. ZTD differentiation

The Canary Islands has a total area of about 7493 km^2, and the meteorological characteristics in each island are similar because the conditions of temperature, pressure, and relative humidity have the same variation pattern with time (*Cropper et al., 2014*; *Alonso-Pérez et al., 2021*). However, local phenomena, such as evaporation, wind movement, and water vapor emission from volcanoes, may cause different patterns of variation at any given time. Figure 5 shows the difference in values of water vapor content, which is a factor affecting the meteorological characteristics of an area.

The variations of *ZTD* and *PWV* values is associated with the difference in the height of the stations. As shown in Table 1, the LPAL station, which is in the highlands, has a higher elevation than the MAZO station on the same island. In addition, GOM1 and GOME, located on La Gomera Island, have elevations at 48.764 and 114.915 m, respectively. A higher place, such as the GNSS station, has decreased water vapor content, leading to reduced tropospheric delay value. A comparison of *ZTD* values between two stations located in different areas using Interim ERA5 reanalysis data from ECMWF via a differentiation analysis method showed that the approach correctly demonstrated Sakurajima 2014 activity in four cases out of five (*Cegla et al., 2022*).

The *ZTD* values for the MAZO and LPAL stations located on La Palma Island, where the eruption occurred, are different from those at the GOM1 station, located on La Gomera Island. The differences are shown in Fig. 5. The differences in the *ZTD* values between MAZO and GOM1, and LPAL and GOM1 stations were also analyzed to determine the significance of the deviations at the stations around the eruption site. Our findings show

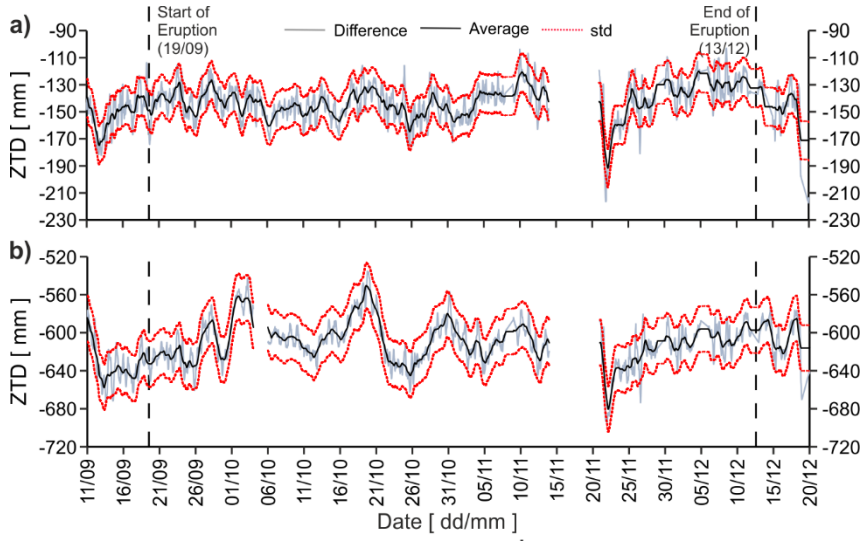

Fig. 5. Differences of the zenith tropospheric delay (*ZTD*) values between **a)** MAZO and GOM1 and **b)** LPAL and GOM1 stations; *std* represents standard deviation (below and above the average values).

Table 1. Ellipsoidal height of the GNSS stations used in the study.

GNSS Station	Location	WGS84 Ellipsoid Height [m]
MAZO	La Palma Island	526.238
LPAL	La Palma Island	2199.219
GOM1	La Gomera Island	48.764
GOME	La Gomera Island	114.915

that the difference in the *ZTD* values between MAZO and GOM1 exceeded one standard deviation (*std*) at several instances. Meanwhile, there was a difference of less than one *std* a few hours after the eruption on 19th September 2021, indicating a decrease in *ZTD* values at the MAZO station. During this period, hot clouds are more likely to spread for several kilometers to reach the station, causing the density of the troposphere to be stretched and resulting in less delay in GNSS signals when passing through the troposphere (*Akilan et al., 2019*).

3.1.3. ZTD comparison (2020 vs 2021)

The *ZTD* values during the eruption period (September–December 2021) are also compared with values for similar period in 2020. Comparison of the *ZTD* values for GNSS stations MAZO and LPAL, located on La Palma Island, are presented in Fig. 6. In the fall of 2020, the *ZTD* values showed higher variations compared to 2021. These variations indicated that the fluctuations observed in 2020 were strongly influenced by higher water

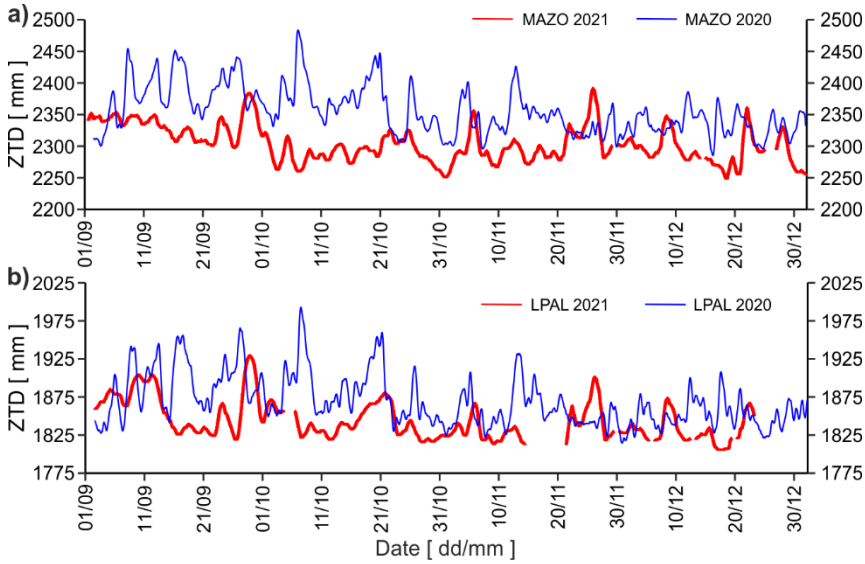

Fig. 6. Zenith tropospheric delay (*ZTD*) values for September–December 2021 and 2020 at **a)** MAZO and **b)** LPAL stations.

vapor levels and more intense rain phenomena, from early fall until the end of 2020. In contrast, the lower fluctuations in *ZTD* values during the fall of 2021 suggested a potential effect due to the eruption of Cumbre Vieja.

3.2. Precipitable water vapor

3.2.1. PWV results at two stations

The *PWV* parameter, which is one of the major atmospheric components of the troposphere, also increased through a similar pattern in the same period (Fig. 7). This indicates that the GNSS delay in the troposphere was influenced by the variations in the wet component, which is water vapor in this case. This was observed through the increase in water vapor content in the atmosphere approximately 2 days after the initial eruption.

Several studies have attempted to measure water vapor emission by evaluating the radiation scattering on water droplets suspended in plumes of volcanic gas (*Girona et al., 2015*; *Pering et al., 2017*). These techniques related the scattering efficiency of water droplets in a volcanic gas plume with the overflow of precipitable water or total column water vapor. They have assumed that water vapor is attracted by the volcanic ash from the eruption. The data obtained from NASA Aerosol Robotic Network (AERONET) showed a significant increase in aerosol concentrations 3 days after the eruption, as indicated by the increasing trend of the *AOD* value from 25th September to 3rd October 2021 (Fig. 8). This increase in *AOD* values is directly proportional to the increase in water vapor content during the same date range.

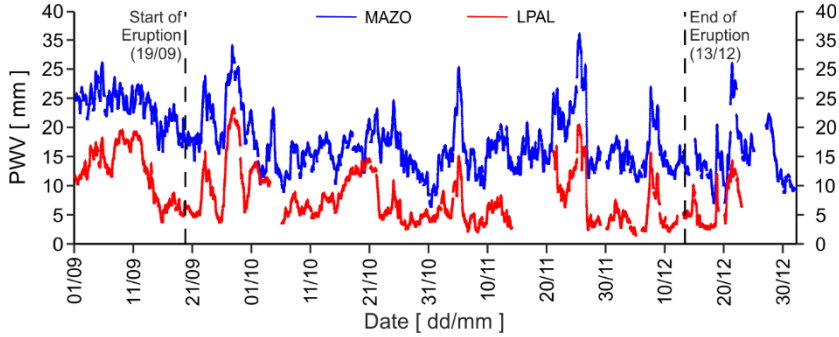

Fig. 7. Precipitable water vapor (*PWV*) content at the MAZO and LPAL stations.

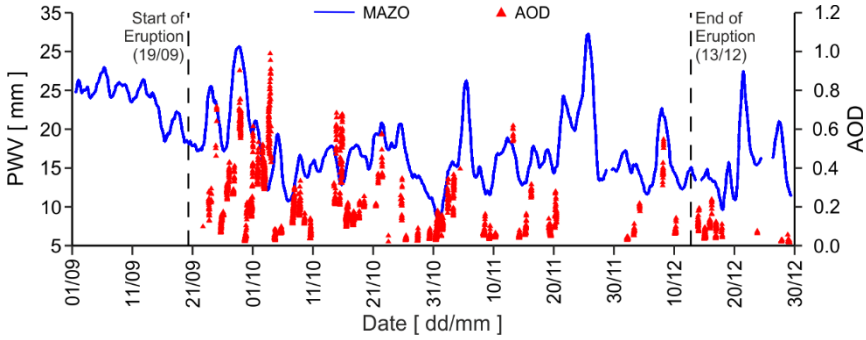

Fig. 8. Precipitable water vapor (*PWV*) content at the nearest station MAZO and aerosol optical depth (*AOD*) at the NASA AERONET ground station.

The wavelengths on the stereoscopy used for the corresponding *AOD* values are generally used to measure the vertical column density of SO_2 content, which is one of the dominant ingredients in volcanic eruptions, and were observed at 340 and 380 nm. The correlation between water vapor and aerosol contents, as determined through the calculation of the correlation coefficient between the two variables during the eruption period, showed a positive value of 0.46.

The increase in *PWV* value as well as the aerosol content indicates a direct impact on the meteorological conditions of La Palma Island, probably because the ash particles released during the eruption process attract or collect water vapor in the atmosphere. As shown in Fig. 7, the increase in water vapor content (21st–24th September and 26th–29th September 2021) also indicates the dominance of water vapor content released in the strombolian-type eruption.

3.3. PWV and radiosonde data

Radiosonde data used for comparison were obtained from Guimar–Tenerife Observations from atmospheric sounding station number 60018 on Tenerife Island, which

is still part of the Canary Islands. The station is approximately 150 km from Mount Cumbre Vieja, indicating that their weather characteristics are practically the same.

As shown in Fig. 9, the precipitable water value decreased shortly after the initial eruption and tended to stagnate until 22nd–23rd September. This also indicates the possibility of a hot cloud spreading to several tens of kilometers.

Water vapor content usually decreases drastically immediately after heavy rain. This indicates that the significant reduction in water vapor content recorded during the eruption was most likely due to the heavy rains in the Canary Islands region. According to the four *PWV* time-series graphs at four GNSS stations in La Palma and La Gomera (Fig. 10), the most drastic decline in water vapor content was observed for 29th September, 5th–6th November, 27th November, 2nd–3rd December and 9th December. Note that the reduction is directly proportional to weather observation data retrieved from La Palma Airport (*https://aviationweather.gov/*), which showed the occurrence of moderate to heavy rain 1–2 days before the decline in water vapor.

Figure 11 shows that the *PWV* content at the MAZO station has a fairly strong correlation with the water vapor data from the Tenerife radiosonde. The Pearson correlation coefficient *r* of 0.8993 indicates similar meteorological characteristics at both locations for

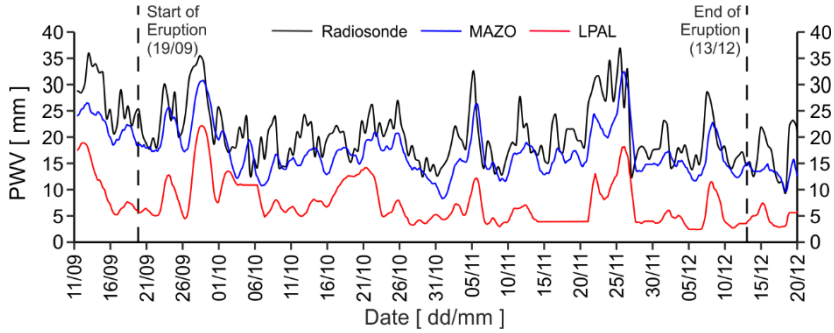

Fig. 9. Precipitable water vapor (*PWV*) content at MAZO and LPAL stations along with water vapor from radiosonde on Tenerife Island.

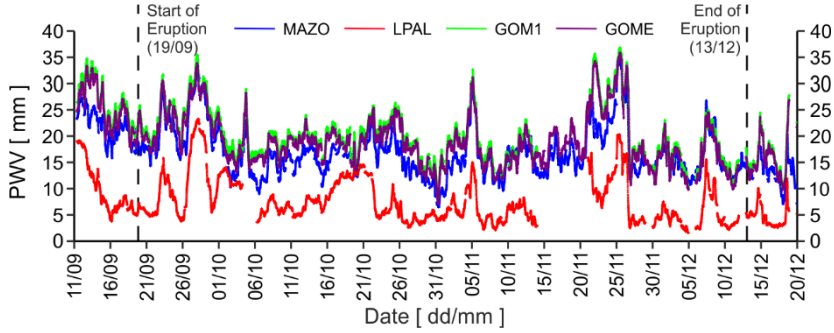

Fig. 10. Precipitable water vapor (*PWV*) content at 4 stations on La Palma and La Gomera islands.

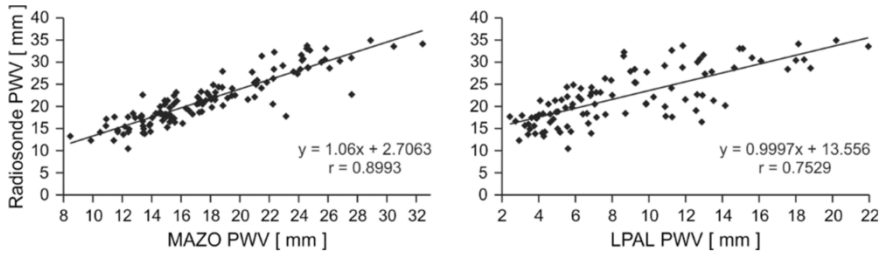

Fig. 11. Correlation between precipitable water vapor (*PWV*) content from radiosonde station in Tenerife and from the GNSS MAZO and LPAL stations (September–December 2021); *r* stands for the Pearson correlation coefficient.

most of the autumn or eruption period. Meanwhile, a lower correlation of 0.7529 was recorded between the *PWV* at the LPAL station and the Tenerife radiosonde due to the difference in altitude of the LPAL station, which is more than 2000 m above sea level. This led to lower *PWV* content, which was not varied significantly in time-series during the eruption period.

3.3.1. PWV comparison (2020 vs 2021)

In this section we compare *PWV* values observed at La Palma for the fall of 2021 and 2020 (Fig. 12). Fluctuations observed in *PWV* showed a change in atmospheric water vapor content and the patterns related to rainfall phenomena. Furthermore, *PWV* behavior in the fall of 2020 at La Palma showed several sharp increases, followed by sharp decreases shortly afterwards. This indicated the occurrence of heavy rainfall, which significantly reduced the amount of water vapor in the atmosphere (*Barindelli et al., 2018*; *Rose et al., 2023*).

In the fall of 2021, *PWV* showed calmer behavior at the beginning of the Cumbre Vieja eruption, and significant fluctuations starting in November until winter. The occurrence of rain during the fall of 2021 was less as compared to 2020, as indicated by the number of rainy days based on weather reports at the La Palma Airport. The number of rainy days in the fall of 2021 was 34, compared to 49 observed in 2020.

3.4. Atmospheric parameters

3.4.1. SO_2 column density

The SO_2 vertical column density data recorded by the TROPOMI Sentinel-5P sensor has a temporal resolution of one day, thereby allowing daily spatial monitoring of SO_2 content in the troposphere. The time series of SO_2 are shown in Fig. 13.

The sensor has sensitive wavelengths at 340 and 380 nm, that are affected by clouds, thereby causing incomplete daily data. However, the plots showed an increase in the SO_2 contents with a significant increase of up to more than 60 mmol m^{-2} in early October for the MAZO and LPAL stations. An increase was also observed on 15^{th}–19^{th} and 29^{th}–31^{st} October, although it was not sufficiently significant at approximately 10 mmol m^{-2}. This phenomenon was caused by the Cumbre Vieja eruption gas and particles carried by the wind in all directions, along with reduced volcanic emissions after the initial eruption. The

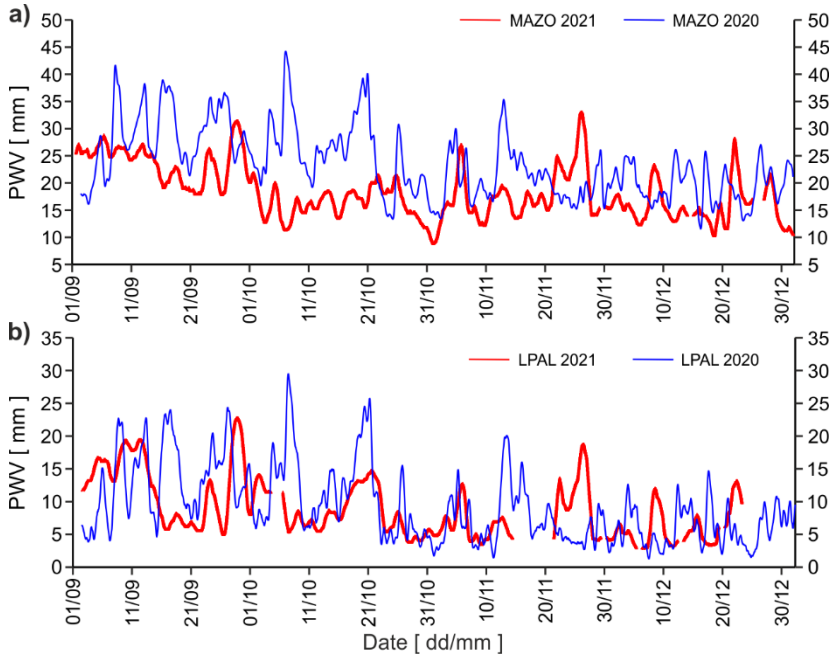

Fig. 12. Precipitable water vapor (*PWV*) for September–December 2021 and 2020 at **a)** MAZO and **b)** LPAL stations.

patterns observed are common in volcanoes, particularly during long periods of eruption. The study by *Bonadonna et al (2015)* and *Poulidis et al (2019)* confirmed the effects of wind dynamics on the atmosphere during the eruption process.

Figure 14 shows SO_2 content in autumn 2020, obtained through Sentinel-5P TROPOMI, presenting a comparison of atmospheric SO_2 content in the absence of eruption. Under normal conditions, the atmosphere maintains a baseline SO_2 content mainly due to human activities. Based on the graph presented in Fig. 14, the highest recorded range did not exceed 4 mmol mm^{-2}. During the fall of 2021, the majority of the SO_2 originated from the eruption activity of the Mount Cumbre Vieja, which occurred for 3 months. Consequently, the highest SO_2 range could reach more than 120 mmol mm^{-2} in the eruption center.

3.4.2. UV aerosol index

The *UVAI* or *AAI* used wavelengths in Rayleigh scattering in the UV spectral range to present the ratio or difference between the observed and modeled reflectance. A positive value indicates the presence of UV-absorbing aerosols, such as dust, smoke, and volcanic ash (in this case). As shown in Fig. 15, the index values in the pixels corresponding to the three GNSS stations has the same pattern as the tropospheric delay and *PWV* values obtained from GNSS observations at the beginning of the eruption from around 20th September to 1st October.

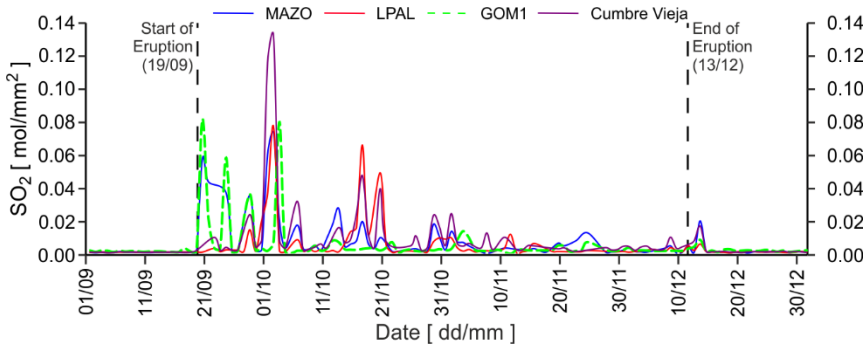

Fig. 13. Verical column density of SO_2 at locations corresponding to MAZO, LPAL and GOM1 stations, and Mount Cumbre Vieja (September–December 2021).

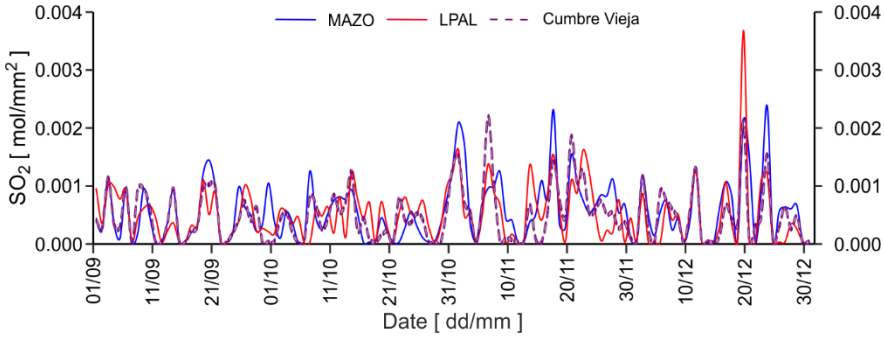

Fig. 14. Verical column density SO_2 at locations corresponding to MAZO and LPAL stations, and Mount Cumbre Vieja (September–December 2020).

As shown in Fig. 16, the MAZO station, which is the closest station to the eruption point, experienced a positive, and high aerosol index value during the period. This finding shows that the obtained reflectance data is much larger than the model data. Therefore, the high value may be influenced by volcanic ash. The findings also suggest that water vapor was produced from the Cumbre Vieja eruption and bound in the aerosol content because the pattern of variation is the same as the *PWV* and *ZTD* content recorded at the beginning of the eruption.

The *ZTD* and *UVAI* values at LPAL and GOM1 stations from 19th September to 2nd October 2021, also have the same increasing trend, as shown in Fig. 17.

Figure 18 shows the UV aerosol index for the same period (13th September to 13th October 2020) at MAZO, LPAL, and GOM1. Compared to 2021, the aerosol index in 2020 did not provide significant fluctuations due to the absence of eruption activity. Consequently, the aerosols in the atmosphere were mostly sourced from mineral dust particles, urban smog, vehicle exhaust, and other sources associated with natural and human activities.

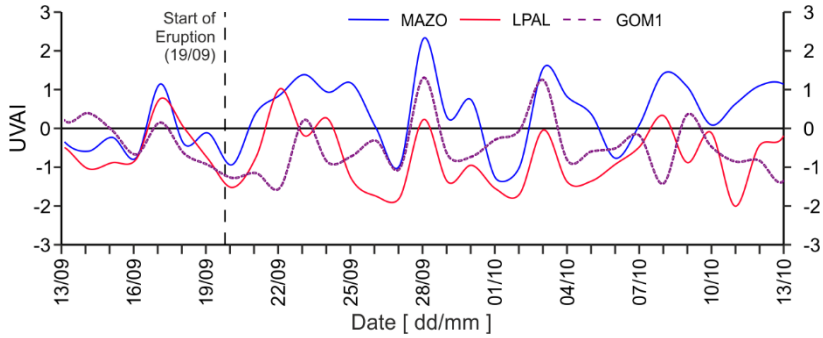

Fig. 15. UV aerosol index (*UVAI*) from TROPOMI Sentinel-5P at locations corresponding to the MAZO, LPAL, and GOM1 stations from 13th September to 13th October 2021.

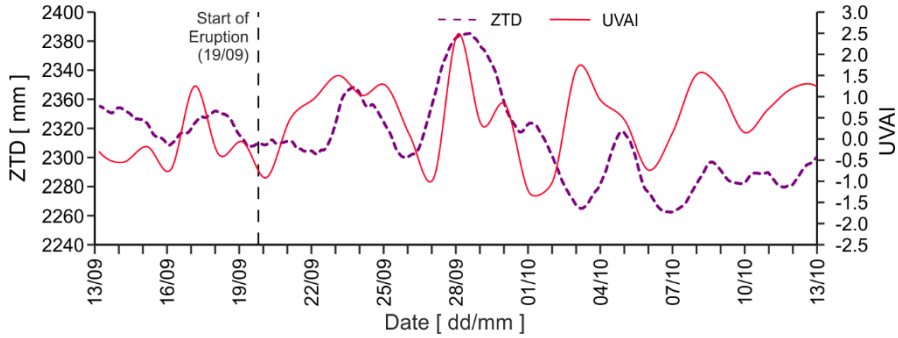

Fig. 16. Zenith tropospheric delay (*ZTD*) and UV aerosol index (*UVAI*) at the MAZO station from 13th September to 13th October 2021.

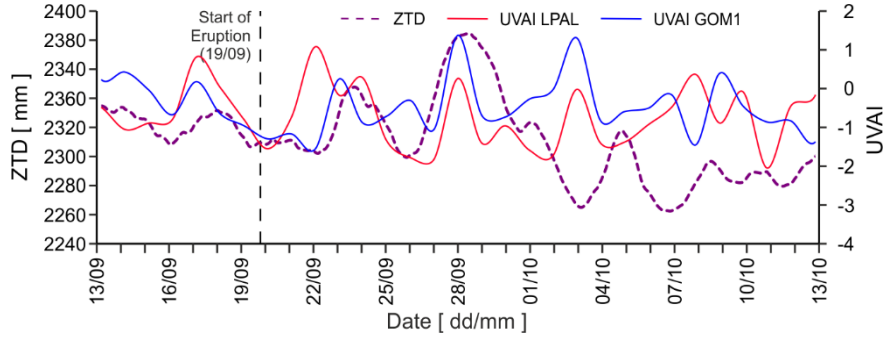

Fig. 17. Average of zenith tropospheric delay (*ZTD*) at LPAL and GOM1 stations and UV aerosol index (*UVAI*) at the two stations from 13th September to 13th October 2021.

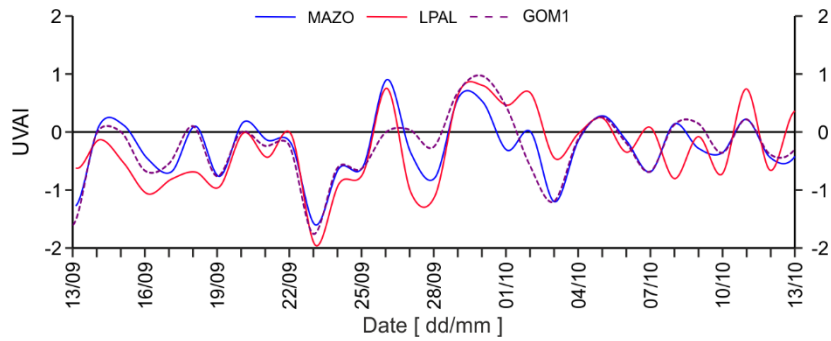

Fig. 18. UV aerosol index (*UVAI*) from TROPOMI Sentinel-5P at locations corresponding to MAZO, LPAL, and GOM1 stations from 13th September to 13th October 2020.

3.4.3. Land surface temperature

MODIS data were used to identify surface temperatures during the eruption period. The land surface temperatue (T_S) is affected by cloud cover and may lead to some hiatuses at any given time. The northern subtropical region usually enters autumn in September 2021, indicating that the surface temperature normally drops continuously until winter arrives in December 2021.

Figure 19 (September–December 2021) and Fig. 20 (September–December 2020) show the MODIS T_s data at locations corresponding to the three stations closest to the eruption. The temperature variations of the pixels corresponding to the GOM1 station fluctuate during the eruption period. The temperature was expected to drop in early autumn, but instead it was observed to increase at the station, from 37.49°C on 25th September to 40.05°C on 18th October. The insignificant increase and decrease in surface temperature indicate subsequent fluctuations in surface temperature. However, hiatuses were observed at the MAZO station on many days, with the only significant increases at 36.17°C and 37.17°C, observed on 2nd and 18th October, respectively. Meanwhile, the increase in temperature at the LPAL station was identified on 20th September, which is the day after the initial eruption, with a daily surface temperature of 28.89°C. This value is quite high because the station is located at an altitude of more than 2000 m a.s.l. Another increase was identified on 2nd–8th October, with fluctuations that exceeded 30°C. The same trend was observed at the GOM1 station.

The comparison with the same period in 2020 (Fig. 20) showed the effect of the eruptions on the fluctuations recorded in T_s on the Canary Islands. Many blank data with respect to daily surface temperatures were found between September and December 2021, and the average value of 25.16°C recorded at the MAZO station was observed to be higher than 25.00°C for the same period in 2020. A similar trend was also discovered at the GOM1 station with 29.92°C and 28.66°C for the respective periods.

The above findings indicate that the eruption period significantly affected the surface temperature, as indicated by the extreme values observed up to the winter period in Europe, i.e., December 2020. However, the available data indicate that some increases in temperature were recorded at the beginning of the eruption.

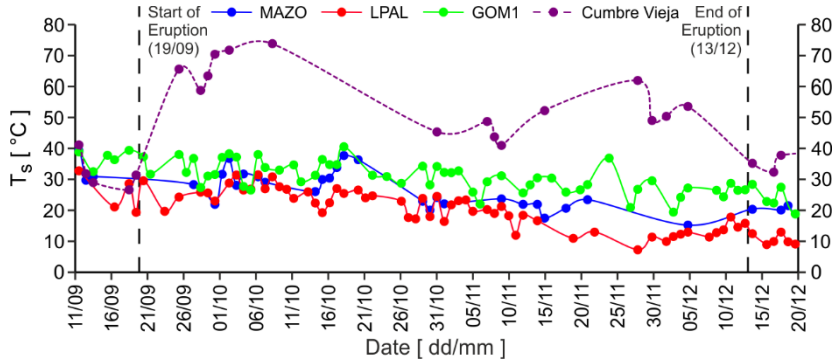

Fig. 19. Land surface temperature (T_S) from MODIS satellite 1 × 1 km image data at the eruption site and three GNSS stations during the 2021 eruption period.

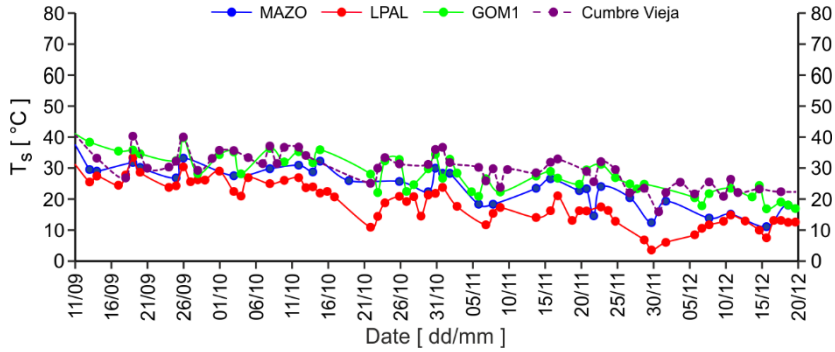

Fig. 20. The same as in Fig. 19, but for 2020.

3.5. Correlation of water vapor with other parameters

The produced time-series graphs were combined into one frame based on the computed parameters (Fig. 21). As shown here, the dotted lines at the beginning and the end indicate the beginning and end of the eruption at Cumbre Vieja, respectively.

Table 2 shows the correlation coefficients between variables at the three GNSS stations, including MAZO, and LPAL on La Palma Island as well as GOM1 on La Gomera Island. According to observations from these stations, the *PWV*, and *ZTD* have correlation coefficient values above 0.980 because the *ZTD* values are generally influenced by variations in *PWV* and the hydrostatic delay value, which tends to be constant over a long period.

After the eruption, both the MAZO and LPAL stations showed fluctuating and then significantly increased values of *ZTD* and *PWV*. The increase in water vapor at the beginning of the eruption, which coincided with the increase in SO_2 content, was probably caused by water vapor emissions from the Cumbre Vieja eruption. Eruptions produced large water vapor emissions that carry volcanic ash particles from the eruption vent to the

atmosphere (*Bryan et al., 2017*; *Kern et al., 2017*). The potential for condensation increases as water vapor rises to the upper and cooler columns of the troposphere (*Bryan et al., 2017*). This probably caused the highest fluctuations and increases in temperature at the beginning of the Cumbre Vieja eruption.

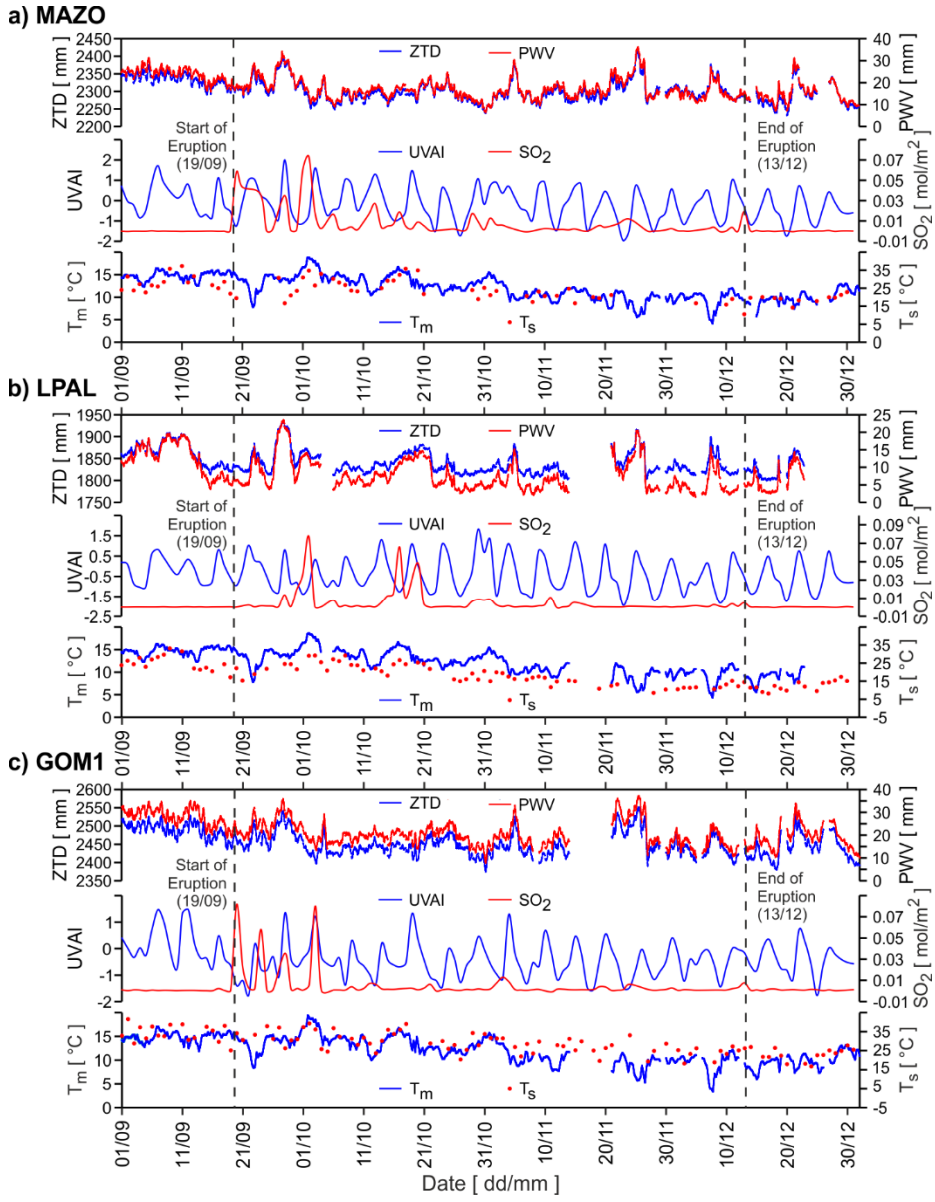

Fig. 21. A composite figure of several atmospheric parameters corresponding to the locations of the **a)** MAZO, **b)** LPAL, and **c)** GOM1 GNSS stations. See text for the meaning of the parameters.

Table 2. Correlation coefficients between atmospheric parameters at locations corresponding to different GNSS stations. See text for the meaning of the parameters. Values in bold are different from 0 with a significance level $\alpha = 0.05$.

Variable	*ZTD* (GNSS)	*PWV* (GNSS)	SO_2 (S5P)	*UVAI* (S5P)	T_m (GNSS)	T_s (MODIS)	*PWV* (Sounding)
MAZO GNSS Station							
ZTD (GNSS)	**1**	**0.987**	–0.132	0.218	0.154	0.110	**0.875**
PWV (GNSS)	**0.987**	**1**	–0.126	0.204	0.186	0.178	**0.899**
SO_2 (S5P)	–0.132	–0.126	**1**	–0.142	**0.374**	0.155	–0.110
UVAI (S5P)	0.218	0.204	–0.142	**1**	0.094	–0.005	0.200
T_m (GNSS)	0.154	0.186	**0.374**	0.094	**1**	**0.684**	0.128
T_s (MODIS)	0.110	0.178	0.155	–0.005	**0.684**	**1**	0.150
PWV (Sounding)	**0.875**	**0.899**	–0.110	0.200	0.128	0.150	**1**
LPAL GNSS Station							
ZTD (GNSS)	**1**	**0.980**	0.225	0.197	**0.334**	**0.602**	**0.744**
PWV (GNSS)	**0.980**	**1**	**0.232**	0.216	**0.370**	**0.646**	**0.752**
SO_2 (S5P)	0.225	**0.232**	**1**	–0.027	**0.333**	**0.278**	0.209
UVAI (S5P)	0.197	0.216	–0.027	**1**	0.191	0.212	0.097
T_m (GNSS)	**0.334**	**0.370**	**0.333**	0.191	**1**	**0.808**	**0.354**
T_s (MODIS)	**0.602**	**0.646**	**0.278**	0.212	**0.808**	**1**	**0.498**
PWV (Sounding)	**0.744**	**0.753**	0.109	0.097	**0.254**	**0.498**	1
GPM1 GNSS Station							
ZTD (GNSS)	**1**	**0.982**	–0.026	**0.325**	0.193	**0.263**	**0.929**
PWV (GNSS)	**0.982**	**1**	–0.024	**0.378**	**0.269**	**0.341**	**0.937**
SO_2 (S5P)	–0.026	–0.024	**1**	0.075	0.186	0.153	–0.031
UVAI (S5P)	**0.325**	**0.378**	0.075	**1**	**0.362**	**0.243**	**0.328**
T_m (GNSS)	0.193	**0.269**	0.186	**0.362**	**1**	**0.710**	0.251
T_s (MODIS)	**0.263**	**0.341**	0.153	**0.243**	**0.710**	**1**	**0.322**
PWV (Sounding)	**0.929**	**0.937**	–0.031	**0.328**	0.251	**0.322**	**1**

The increase in *ZTD* and *PWV* coincided with the increase in SO_2 in MAZO from late September to early October. The T_s values show the same increase and decrease patterns as the GNSS T_m data. Both experienced the highest increase on 1st–3rd October, which coincided with a drastic increase in the SO_2 content in MAZO. This period shows a high concentration of SO_2 and creates hot clouds in the troposphere.

As shown in Fig. 21b, the atmospheric parameters at the LPAL station location show a relatively similar pattern to the graph for the MAZO station location. The location of the station in the highlands results in dynamic weather conditions; thus, the water vapor show drastic variations at the station in a fairly short period. Similar to MAZO, the distribution of SO_2 particles increased in October and then slightly affected the SO_2 content at the station location in November. Surface and average temperatures also fluctuated in October and tended to decrease as winter approached.

The Cumbre Vieja eruption lasted for nearly three months, causing the eruption particles to spread for hundreds of kilometers in a short time. The GOM1 station, which is located on a different island and is more than 100 km from the center of the eruption, also experienced an increase in SO_2 content in the atmosphere. As shown in Fig. 21c, the SO_2 content showed highest activity in October and then decreased in November. The characteristics of *ZTD*, *PWV*, T_S, and mean temperature also tend to be similar to the characteristics observed at the two previous station locations.

The *PWV* and *ZTD* data at MAZO show low correlation with other lower atmosphere variables, especially with the vertical column density SO_2 content, with the correlation coefficient of –0.132 and –0.126, respectively. Their correlation with *UVAI*, T_m and T_S is generally less than 0.2. Meanwhile, T_S showed a slightly higher correlation with SO_2 content (0.374). Mean temperature T_m and T_S also showed a fairly high correlation of 0.684. This finding reflects a relationship between the surface and the average temperature of the total column in the troposphere.

Our findings also show that T_S is correlated with *PWV* and *ZTD* (0.602 and 0.646, respectively), and the SO_2 content is correlates with T_S with a coefficient of 0.278, which is considered to be quite low. Meanwhile, T_S and T_m at the location have a correlation coefficient of 0.808. This indicates that surface temperature can greatly influence the average tropospheric temperature.

The tropospheric variable at the GOM1 station is relatively similar to that at LPAL, although it has a generally lower correlation value. *ZTD* and *PWV* contents were positively correlated with *UVAI* but showed no correlation with SO_2 content. The correlation between *PWV* and T_S variables is also quite low at 0.341, which is smaller than the values of the two variables at the LPAL station but higher than that at the MAZO station. Moreover, the T_S is highly correlated with mean temperature as also observed in LPAL. This indicates the possibility that the surface temperature greatly influences the average tropospheric temperature.

The observed correlation coefficients are in general rather low. The only exception is the correlation between the *PWV*/*ZTD* and the T_S and GNSS mean temperature values. The higher correlation at LPAL station (Table 2) is generally due to the characteristics of the troposphere. The higher is the altitude (lower tropospheric pressure), the higher is the correlation between temperature and humidity. This is due to the frictional increase in humidity up to 6% as the temperature rises at an altitude higher than 2000 m (*Sun et al., 1996*). It is known that the LPAL station is in the northern highlands of La Palma Island. The relatively higher correlation at the LPAL station represents this phenomenon.

Table 2 also shows the correlation with water vapor data obtained using radiosonde. The correlation values do not show better results than the GNSS data. This is due to the relatively far distance of the radiosonde station (about 150 km from the eruption center). Based on several previous studies, it is known that the farther the radiosonde station is from the study site, the less representative it is for the study site, for which atmospheric information is desired (*Ning and Elgered, 2012*; *Ning et al., 2013*; *Bonafoni et al., 2013*). The characteristics of climate similarity cause similarities in pressure and temperature fluctuations in the atmosphere despite the relative distance (*Šebela and Turk, 2011*; *Rummukainen, 2012*). However, dynamic atmospheric conditions will cause differences in

Table 3. Correlation coefficient between *PWV* and SO_2, *UVAI and* T_s from 19th September to 31st October 2021 for different GNSS stations. Values in bold are different from 0 with a significance level $\alpha = 0.05$.

	GNSS Station		
	MAZO	LPAL	GOM1
PWV vs SO_2	**0.292**	**0.489**	**0.301**
PWV vs *UVAI*	**0.505**	**0.433**	**0.586**
PWV vs T_s	**0.397**	**0.785**	**0.514**

weather conditions such as rain, fog, and volcanic ash (*Wang et al., 2017*; *Butwin et al., 2020*). Thus, although radiosonde data are more in line with the real atmospheric situation, they do not highly correlated to the weather situation at locations relatively far from the radiosonde station (Fig. 11 and Table 2).

To further see whether the intensity of the eruption and meteorological activity affect the correlation results for the 3 months of the eruption period, the correlation coefficient for a more specific period is also calculated. The correlation coefficients between *PWV* on one hand, and SO_2, *UVAI* and T_s on the other, were calculated for the period from 19th September to 31st October 2021 (Table 3), when the eruption intensity was high.

Table 3 shows that the correlation coefficients for the period from 19th September to 31st October 2021 are higher than those for the entire eruption period (19th September to 13th December 2021). This correlation calculation is based on eruption conditions which generally have a high intensity from the beginning of the eruption to the end of October (based on SO_2 monitoring in Fig. 13), as well as a decrease in SO_2 intensity in early November until it approaches winter. In addition, these calculations are also based on meteorological conditions during the eruption period. Rain intensity at the beginning of the eruption until the end of October is generally low (Figs 22–23).

4. DISCUSSION

This study showed that the water vapor content generated from GNSS data had varied fluctuations during the Cumbre Vieja eruption period in the autumn of 2021. The *PWV* variations in this study directly affected the tropospheric delay (*ZTD*) by 96%–99%, indicating that water vapor content influences the variation in tropospheric delay in the study area. The increase and decrease of *ZTD* are generally influenced by the fluctuation of tropospheric wet component represented by *PWV* content (*Zhao et al., 2018*; *Wei et al., 2021*; *Rose et al., 2023*). In the context of eruption phenomena, hot tropospheric conditions at the beginning of the eruption period cause the atmospheric density to decrease, so that GNSS signal propagation becomes faster and signal delay in the troposphere becomes lower (*Akilan et al., 2019*). A significant burst of volcanic particles into the atmosphere can affect the GNSS signal delay in the troposphere by increasing *ZTD* (*Larson, 2013*; *Grapenthin et*

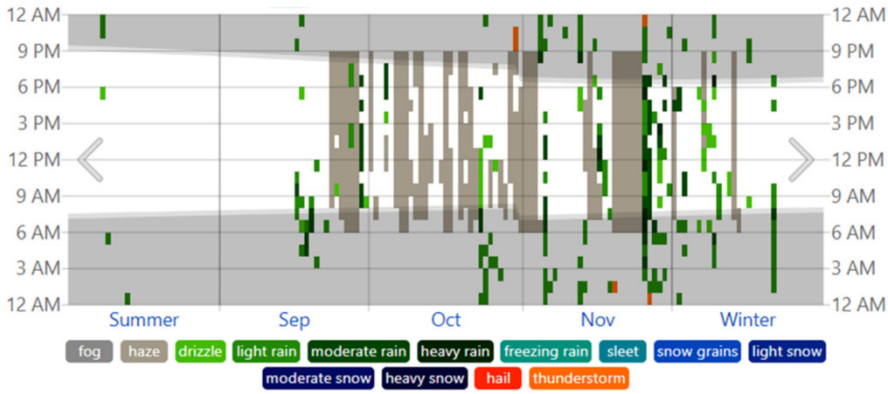

Fig. 22. Observed weather in the fall of 2021 in La Palma from the weather reports at the La Palma Airport (*https://weatherspark.com/h/y/149923/2021/Historical-Weather-during-2021-at-La-Palma-Airport-Spain#Figures-ObservedWeather*).

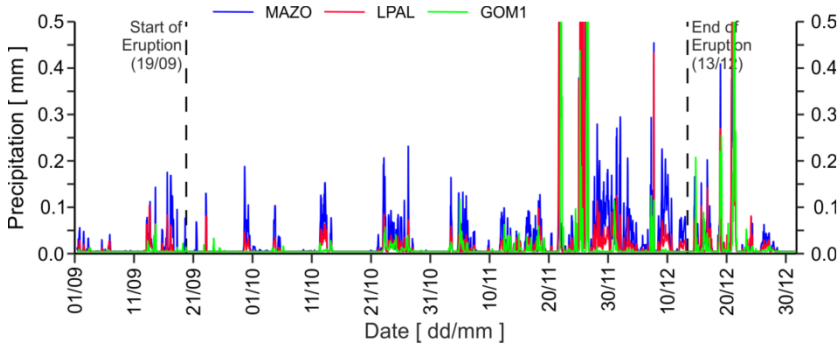

Fig. 23. Hourly precipitation at 3 GNSS stations according to the European Center for Medium-Range Weather Forecasts (ECMWF).

al., 2013; *Cegla et al., 2022*). This reflects the impact of the eruption on tropospheric parameters in GNSS monitoring.

The fluctuating water vapor content shows the characteristics of autumn in the Canary Islands region, where weather conditions are dominated by rain, specifically in November toward winter 2021, as shown by the La Palma weather reports in Fig. 22. This result is consistent with the findings of several studies that high rainfall is directly proportional to the extreme intensity of rain or weather in an area (*Bryan et al., 2017*; *Kern et al., 2017*; *Cahyadi et al., 2017, 2023*).

Cumbre Vieja experienced a high-intensity eruption from late September to late October 2021 (as shown in Fig. 13). After that period until the end of the eruption activity in mid-December, the eruption intensity decreased, as indicated by the smaller SO_2 content in the atmosphere. This is inversely proportional to the increasing intensity of rain in early November until it approaches winter. Additional supporting data were obtained in the form

of rainfall data sourced from the ECMWF ERA5 climate reanalysis, which allows hourly interval time-series data. Data were extracted for the locations of 3 GNSS stations from 1st September to 31st December 2021 (Fig. 23).

It can be seen from Fig. 23 that the rain intensity from the beginning of the eruption to the end of October was generally not too high. While in early November to the end of December the rain intensity was relatively higher than the previous period. During heavy rains, the propagation of GNSS signals in the troposphere were more influenced by high water vapor content, so that the correlation with SO_2 content has the potential to be less significant. In addition, the presence of rainwater and SO_2 in the atmosphere will cause a chemical reaction in the atmosphere, i.e., the process of dissolving SO_2 with water vapor in the atmosphere to form sulfuric acid (*Glaze et al., 1997*; *McGouldrick et al., 2011*).

The SO_2 content was observed to have dominated the atmosphere of La Palma from the beginning of the eruption to the end of October 2021 and started decreasing in all three GNSS stations from November to December 2021 (Fig. 24). Moreover, the distribution of SO_2 in all directions by the wind reduced its vertical column density. As indicated in Fig. 21, the weather conditions and higher rainfall intensity initiated the decline of aerosol particles and SO_2 vertical column density due to eruption and the low correlation between *PWV* and SO_2 in the three stations. This is also in line with the findings of a previous study (*Guo et al., 2021*). Values of *ZTD* and *PWV* exhibited low correlation with atmospheric particle content due to uncertain weather conditions (*Wei et al., 2021*). Furthermore, the location, and altitude of the station also affected the correlation of *ZTD* and *PWV* with aerosol and SO_2 content. The correlation between these parameters for stations located in higher altitude tends to be higher under fluctuating atmospheric conditions (*Wei et al., 2021*; *Kundu et al., 2022*; *Cahyadi et al., 2024*).

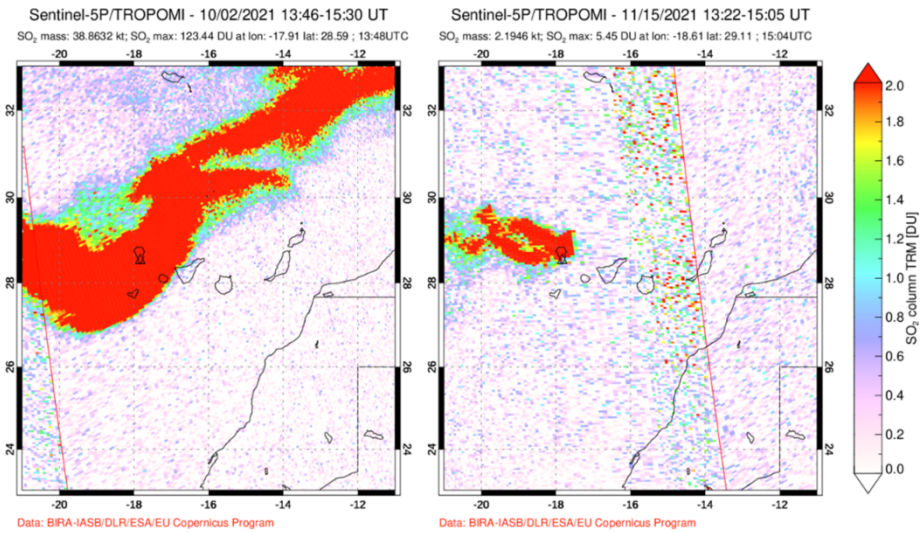

Fig. 24. Distribution of vertical column density of SO_2 in the Canary Islands; **left:** 2nd October 2021, **right:** 15th November 2021 (*https://so2.gsfc.nasa.gov*).

Meanwhile, the correlation coefficient between mean temperature (T_m - GNSS) and T_s at the three GNSS stations ranged from 0.68 to 0.81. In the early eruption period, i.e. between late September and early October 2021 (Fig. 24), both these parameters showed increased values that are directly proportional to the increase in SO_2 content. This indicates high eruptive activity, which led to higher surface and tropospheric average temperatures. Nevertheless, this pattern was not repeated in November toward winter when both T_m and T_s were reduced.

5. CONCLUSIONS

The Cumbre Vieja 2021 eruption period was characterized by changes in water vapor that stagnated for a few days before the actual eruption, followed by a fluctuation during the period that coincided with autumn in Europe when temperatures in the troposphere continued to decline toward winter. Similarly, high intensity of SO_2 content dominated the atmospheric particles in October 2021 due to the volcanic eruption. The eruption period, which coincided with the autumn period, was majorly characterized by water vapor content due to heavy rain in early November to near the beginning of winter. The GNSS parameters did not correlate with the SO_2 content or aerosol particles for the entire eruption period. However, the correlation between GNSS and sensing parameters were relatively higher when Cumbre Vieja experienced high-intensity eruption, where the SO_2 content were higher, and the rainfall intensity were lower. These findings also showed that the surface and average tropospheric temperatures at the three GNSS station locations have an average correlation coefficient above 0.7. This indicates that surface temperature might greatly influence the average tropospheric temperature.

Code and Data Availability: The RINEX Observation and Troposphere Data are available in UNAVCO GAGE Facility Data Center (https://www.unavco.org/data/gps-gnss/gps-gnss.html). All remote sensing data in this research are available in Google Earth Engine datasets trough cloud computing.

Author Contributions: MNC led the problem and topics identification and analysis. All co-authors equally contributed to the design of the study and the interpretation of the results. AB and SA conducted the analysis of precipitable water vapor and rainfall characteristics, supported by SAHS. AW and MR conducted the introduction and analysis of natural hazards, supported by ZH. EYH conducted the analysis for remote sensing parameters and tropospheric delay, supported by PM and ASAL.

Acknowledgements: The authors are grateful to the Upgrade Tugas Akhir-Publication Writing-IPR Incentive Program (PPHKI) 2024 for the financial support of this study.

References

Akilan A., Azeez K.A., Schuh H., Padhy S. and Kotluri S.K., 2019. Perturbations in atmospheric gaseous components over coastal Antarctica detected in GPS signals and its natural origin to volcanic eruption. *Polar Sci.*, **19**, 69–76

Alonso-Pérez S., López-Solano J., Rodríguez-Mayor L. and Márquez-Martinón J.M., 2021. Evaluation of the tourism climate index in the Canary Islands. *Sustainability*, **13**, Art.No. 7042, https://doi.org/10.3390/su13137042

Barindelli S., Realini E., Venuti G., Fermi A. and Gatti A., 2018. Detection of water vapor time variations associated with heavy rain in northern Italy by geodetic and low-cost GNSS receivers. *Earth Planets Space*, **70**, Art.No. 28, https://doi.org/10.1186/s40623-018-0795-7

Bennis K.L. and Venzke E. (Eds), 2021. *Report on La Palma (Spain)*. *Bulletin of the Global Volcanism Network*, **47**. Smithsonian Institution, https://doi.org/10.5479/si.GVP.BGVN202202-383010

Bevis M., Businger S., Chiswell S., Herring T.A., Anthes R.A., Rocken C. and Ware R.H., 1994. GPS meteorology: Mapping zenith wet delays onto precipitable water. *J. Appl. Meteorol.*, **33**, 379–386

Bevis M., Businger S., Herring T.A., Rocken C., Anthes R.A. and Ware R.H., 1992. GPS meteorology: Remote sensing of atmospheric water vapor using the Global Positioning System. *J. Geophys. Res.-Atmos.*, **97**, 15787–15801

Bonadonna C., Pistolesi M., Cioni R., Degruyter W., Elissondo M. and Baumann V., 2015. Dynamics of wind-affected volcanic plumes: The example of the 2011 Cordón Caulle eruption, Chile. *J. Geophys. Res.-Solid Earth*, **120**, 2242–2261

Bonafoni S., Mazzoni A., Cimini D., Montopoli M., Pierdicca N., Basili P., Ciotti P. and Carlesimo G., 2013. Assessment of water vapor retrievals from a GPS receiver network. *GPS Solut.*, **17**, 475–484

Bryan S., Clarke A., Vanderkluysen L., Groppi C., Paine S., Bliss D.W., Aberle J. and Mauskopf P., 2017. Measuring water vapor and ash in volcanic eruptions with a millimeter-wave radar/imager. *IEEE Trans. Geosci. Remote Sensing*, **55**, 3177–3185

Butwin M.K., von Löwis S., Pfeffer M.A., Dagsson-Waldhauserova P., Thorsson J. and Thorsteinsson T., 2020. Influence of weather conditions on particulate matter suspension following the 2010 Eyjafjallajökull volcanic eruption. *Earth Interact.*, **24**, Art.No. 1, https://doi.org/10.1175/EI-D-20-0006.1

Cahyadi M.N., Audah S., Mutia N. and Aliyan S.A., 2017. Analysis of weather changes in the region of Surabaya in 2015 and 2016 using water vapor data from GPS and terra MODIS satellite image. *AIP Conf. Proc.*, **1857**, Art.No. 080003, ttps://doi.org/10.1063/1.4987097

Cahyadi M.N., Bawasir A., Arief S., Widodo A., Rusli M., Kusumawardani D., RahmawatiY., Martina A., Maulida P. and Lestiana H., 2024. Analysis of the effect of the 2021 Semeru eruption on water vapor content and atmospheric particles using GNSS and remote sensing. *J. Geod. Geodyn*., **15**, 33–41

Carracedo J.C., Troll V.R., Day J.M., Junca M.A., Soler V., Deegan F.M., Perez-Torrado F.J., Gisbert G., Gazel E. Rodriguez-Gonzales A. and Minguez H.A., 2022. The 2021 eruption of the Cumbre Vieja Volcanic Ridge on La Palma, Canary Islands. *Geology Today*, **38**, 94–107, https://doi.org/10.1111/gto.12388

Cegla A., Rohm W., Lasota E. and Biondi R., 2022. Detecting volcanic plume signatures on GNSS signal, based on the 2014 Sakurajima eruption. *Adv. Space Res.*, **69**, 292–307

Cofano A., Cigna F., Santamaria Amato L., Siciliani de Cumis M. and Tapete D., 2021. Exploiting Sentinel-5P TROPOMI and ground sensor data for the detection of volcanic SO_2 plumes and activity in 2018–2021 at Stromboli, Italy. *Sensors*, **21**, Art.No. 6991, https://doi.org/10.3390/s21216991

Cropper T.E. and Hanna E., 2014. An analysis of the climate of Macaronesia, 1865–2012. *Int. J. Climatol.*, **34**, 604–622

Girona T., Costa F. and Schubert G., 2015. Degassing during quiescence as a trigger of magma ascent and volcanic eruptions. *Sci. Rep.*, **5**, Art.No. 18212, https://doi.org/10.1038/srep18212

Glaze L.S., Baloga S.M. and Wilson L., 1997. Transport of atmospheric water vapor by volcanic eruption columns. *J. Geophys. Res.-Atmos.*, **102**, 6099–6108

Grapenthin R., Freymueller J.T. and Kaufman A.M., 2013. Geodetic observations during the 2009 eruption of Redoubt Volcano, Alaska. *J. Volcanol. Geotherm. Res.*, **259**, 115–132

Grapenthin R., Hreinsdottir S. and Van Eaton A.R., 2018. Volcanic hail detected with GPS: The 2011 eruption of Grímsvötn Volcano, Iceland. *Geophys. Res. Lett.*, **45**(22), 12236–12243

Guo M., Zhang H. and Xia P., 2021. Exploration and analysis of the factors influencing GNSS PWV for nowcasting applications. *Adv. Space Res.*, **67**, 3960–3978

Hersbach H., Bell B., Berrisford P., Biavati G., Horányi A., Muñoz Sabater J., Nicolas J., Peubey C., Radu R., Rozum I., Schepers D., Simmons A., Soci C., Dee D. ad Thépaut J-N., 2023. *ERA5 Hourly Data on Single Levels from 1940 to Present.* Copernicus Climate Change Service (C3S) Climate Data Store (CDS), https://doi.org/10.24381/cds.adbb2d47

Karabatić A., 2011. *Precise Point Positioning (PPP) - An Alternative Technique for Ground Based GNSS Troposphere Monitoring.* PhD Thesis. Faculty of Mathematics and Geoinformation, Vienna University of Technology, Vienna, Austria

Kern C., Masias P., Apaza F., Reath K.A. and Platt U., 2017. Remote measurement of high preeruptive water vapor emissions at Sabancaya volcano by passive differential optical absorption spectroscopy. *J. Geophys. Res.-Solid Earth*, **122**, 3540–3564

Kundu B., Panda D., Vissa N.K. and Tyagi B., 2022. Novel 2019 Coronavirus outbreak through the eyes of GNSS signal. *J. Geol. Soc. India*, **98**, 83–87

Lachatre M., Mailler S., Menut L., Cholakian A., Sellitto P., Siour G., Guermazi H., Salerno G. and Giammanco S., 2022. Modelling SO_2 conversion into sulfates in the mid-troposphere with a 3D chemistry-transport model: the case of Mount Etna's eruption on April 12, 2012. *Atmos. Chem. Phys.*, **22**, 13861–13879

Larson K.M., 2013. A new way to detect volcanic plumes. *Geophys. Res. Lett.*, **40**, 2657–2660

McGouldrick K., Toon O.B. and Grinspoon D.H., 2011. Sulfuric acid aerosols in the atmospheres of the terrestrial planets. *Planet. Space Sci.*, **59**, 934–941

Mirabel P. and Katz J.L., 1974. Binary homogeneous nucleation as a mechanism for the formation of aerosols. *J. Chem. Phys.*, **60**, 1138–1144

Ning T. and Elgered G., 2012. Trends in the atmospheric water vapor content from ground-based GPS: The impact of the elevation cutoff angle. *IEEE J. Sel. Top. Appl. Earth Observ. Remote Sens.*, **5**, 744–751

Ning T., Elgered G., Willén U. and Johansson J.M., 2013. Evaluation of the atmospheric water vapor content in a regional climate model using ground-based GPS measurements. *J. Geophys. Res.-Atmos.*, **118**, 329–339

Pering T.D., McGonigle A.J., Tamburello G., Aiuppa A., Bitetto M., Rubino C. and Wilkes T.C., 2017. A novel and inexpensive method for measuring volcanic plume water fluxes at high temporal resolution. *Remote Sens.*, **9**, Art.No. 146, https://doi.org/10.3390/rs9020146

Poulidis A.P., Takemi T. and Iguchi M., 2019. The effect of wind and atmospheric stability on the morphology of volcanic plumes from vulcanian eruptions. *J. Geophys. Res.-Solid Earth*, **124**, 8013–8029

Robock A., 2000. Volcanic eruptions and climate. *Rev. Geophys.*, **38**, 191–219

Rose M.S., Sunil P.S., Zacharia J., Sreejith K.M., Sunda S., Mini V.K., Sunil A.S. and Kumar K.V., 2023. Early detection of heavy rainfall events associated with the monsoon in Kerala, India using GPS derived ZTD and PWV estimates: A case study. *J. Earth Syst. Sci.*, **132**, Art.No. 23, https://doi.org/10.1007/s12040-022-02034-5

Rummukainen M., 2012. Changes in climate and weather extremes in the 21st century. *Wiley Interdiscip. Rev.-Clim. Chang.*, **3**, 115–129, https://doi.org/10.1002/wcc.160

Šebela S. and Turk J., 2011. Local characteristics of Postojna Cave climate, air temperature, and pressure monitoring. *Theor. Appl. Climatol.*, **105**, 371–386

Seeber G., 2003. *Satellite Geodesy: Foundation, Methods, and Application*. Walter de Gruyter, Berlin, Germany

Shinohara H., Aiuppa A., Giudice G., Gurrieri S. and Liuzzo M., 2008. Variation of H_2O/CO_2 and CO_2/SO_2 ratios of volcanic gases discharged by continuous degassing of Mount Etna volcano, Italy. *J. Geophys. Res.-Solid Earth*, **113**, Art.No. B09203, https://doi.org/10.1029/2007JB005185

Sun D.Z. and Held I.M., 1996. A comparison of modeled and observed relationships between interannual variations of water vapor and temperature. *J. Climate*, **9**, 665–675

Wang X., Zhang K., Wu S., He C., Cheng Y. and Li X., 2017. Determination of zenith hydrostatic delay and its impact on GNSS-derived integrated water vapor. *Atmos. Meas. Tech.*, **10**, 2807–2820

Wei P., Xie S., Huang L. and Liu L., 2021. Ingestion of GNSS-derived ZTD and PWV for spatial interpolation of PM2.5 concentration in Central and Southern China. *Int. J. Environ. Res. Publ. Health*, **18**, Art.No. 7931, https://doi.org/10.3390/ijerph18157931

Zhao Q., Yao Y., Yao W.Q. and Li Z., 2018. Near-global GPS-derived PWV and its analysis in the El Niño event of 2014–2016. *J. Atmos. Sol.-Terr. Phys.*, **179**, 69–80